J. Nadarasa, C. Deck, F. Meyer, N. Bourdet, J. S. Raul, R. Willinger

Abstract Retinal haemorrhages appear both in case of traffic accidents, fall cases and in case of child abuse. Their mechanisms are poorly investigated. Existing eye finite-element models are used for very specific purposes and there is a lack of detailed modelling. The aim of this study was to develop a complete infant eye finite-element model to investigate eye injuries after falls. The finite-element model of the eye and surrounding components were generated from dimensions available in the literature and from infant MRI data. A set of five occipital impact experiments on a six weeks old baby dummy was performed on different surfaces and heights. The recorded accelerations were used as inputs for the eye finite-element model to replicate occipital, lateral and frontal impacts. Results from experiments showed that the maximum linear acceleration ranged from 110-687 g (HIC15 values from 150 to 6000). From the simulations, five parameters (Pressure, Von-Mises stress/strain, Principal stress/strain) were computed for all eye components and compared. Focus was put on the retina and results demonstrated that parameter values increase along acceleration and HIC15 values. Moreover in frontal impacts, intra-ocular parameters are higher than in occipital or temporal ones. More documented infant falls will help to establish an injury threshold for retinal haemorrhages to be applied in automotive crash environment.

Keywords eye finite element model, infant fall, retinal haemorrhages

I. INTRODUCTION

For infants, following falls from beds, chairs or from the arms of their carers, haematomas, bone fractures and brain injuries are commonly seen injuries. In some fall cases, medical reports mention retinal haemorrhages (RH). RH consist of retinal blood vessel tearing, which split after a specific strain inducing bleeding in the retina. Nevertheless, RH associated to fractures and brain injuries also lead to the diagnosis of abusive head trauma, as reported in [1] and thus, there is a source of controversy about their appearance and the underlying causes [2-3]. One study reported that RH appear in 17% of fatal head accidents whereas it appears in 89% of abusive head trauma cases [4]. This kind of injury also appears in case of traffic accidents and there is therefore a need to better understand the mechanisms of RH occurrence. The finite-element method is a powerful and widely used tool in different fields, in particular in biomechanics. Few eye finite-element models (FEM) have been developed in the literature for specific purposes: blunt impact studies, effects of blast, eye accommodation studies [5-7].

One of the first eye FEM was developed in [8]. Modelling the sclera, cornea, lens, aqueous and vitreous humors, iris, ciliary body and choroid, the aim was to study the effect of small body impacts on the eye (at 30 m/s and 60 m/s) by comparing maximum strain in the cornea and the sclera with the failure strain obtained from the experiments. A few years later, the model developed in [5] marked a step in eye FEM development as the authors set up a validation protocol for the model. After modelling the whole globe and its inner components (except retina and choroid), eye impact experiments have been conducted on 22 human eyes with airsoft balls, foam pieces and baseballs. The authors proposed a validation of the FEM by comparing visually the deformation of globes in the videos and simulation animation, and comparing areas with maximum stresses with the areas where the globes have split.

In 2005, [9] proposed a model composed of aqueous, vitreous, sclera, optic nerve, fat and orbital wall and published different studies such as eye restraint mechanisms in head impacts [9], shaken baby syndrome SBS outcomes [10], and optic nerve injuries [11]. The authors showed that the fat has a leading role in holding the globe inside the orbit. In their latest article, their study highlighted how blunt object impact can damage the optic nerve head. More recently, [12] published one of the most detailed models: the whole inner globe and orbital components were included. The aim of the study was to understand why RH appear mostly in abusive head trauma cases (shaken baby syndrome) and merely after a low height fall. After performing a shaking and a

J. Nadarasa is a PhD student in Biomechanics at MMB-ICube, University of Strasbourg, France. C. Deck is a Researcher in Biomechanics, F. Meyer is a Researcher in Biomechanics, N. Bourdet is a Researcher in Biomechanics and R. Willinger is Professor of Biomechanics at MMB-ICube, University of Strasbourg, France. J. S. Raul is Professor in Legal Medicine at the Legal Medicine Institute of Strasbourg, France.

45 cm height backward fall simulations with the eye model, a comparison was made between the force sustained in the retina with experimental data on monkey eyes. It showed clearly that the threshold was exceeded during the shaking case and not at all reached in the fall case.
Finally, a study about retinal detachment after blunt impact was published in [13]. The model included all components except the muscles and choroid layer. Retina and choroid contact was experimentally characterized with in vivo testing on rabbit eyes: a value of 340±78 Pa was established. A parametric study with vitreous shear modulus and impact speed was performed and results show that up to 32% of the retina can be detached in some situations.

Among the mentioned studies, only [12] have investigated RH from falls. Furthermore, to study outcomes of impacts, there is a clear need to quantify them in order to accurately reproduce the acceleration sustained by the infant eye during head impacts. Moreover, those FEM failed to model specifically all eye components with their surrounding materials such as orbital fat, muscles and optic nerve. The aim of this study is to overcome the two points by providing a set of experimental dummy impact cases and developing a complete infant eye model with updated material properties. Using experimental results as inputs for the FEM will give first insights on mechanical eye response under multidirectional head impact.

II. MATERIAL AND METHODS

To overcome the objectives, the experimental protocol to precisely define impacts and eye loading is described, followed by a detailed description of the developed eye FEM. The performed simulations and computed parameters are presented at the end of the section.

Experimental Dummy Falls

The dummy used here is called Q0 (Humanetics Europe, Heidelberg, Germany) and represents a six weeks-old newborn, with a mass of 3.46kg, 59.7cm long and linear accelerometers at the center of gravity of the head (Fig. 1 A-B). This dummy was used in 2 different impact situations. The first impact situation consisted of dropping the dummy from a 45 cm height on grass, linoleum and concrete surfaces and from a 130 cm height on concrete surface. Attention was placed on making the dummy land horizontally on the surface. For the second impact situation, a volunteer was asked to impact the occipital area of the dummy head against a wall. Table I summarizes the different impact experiments which lead to head accelerations that can be experienced in fall, car crash or child abuse cases.
The head response was recorded with a high frequency camera (Optronis CR3000x2, 500 fps, Optronics GmbH, Kehl, Germany) and an illustration is proposed in Fig. 1 - C. Here will only the acceleration along the impact direction (X axis) be reported and considered, however the other directions were still recorded in order to check the impact direction properly.

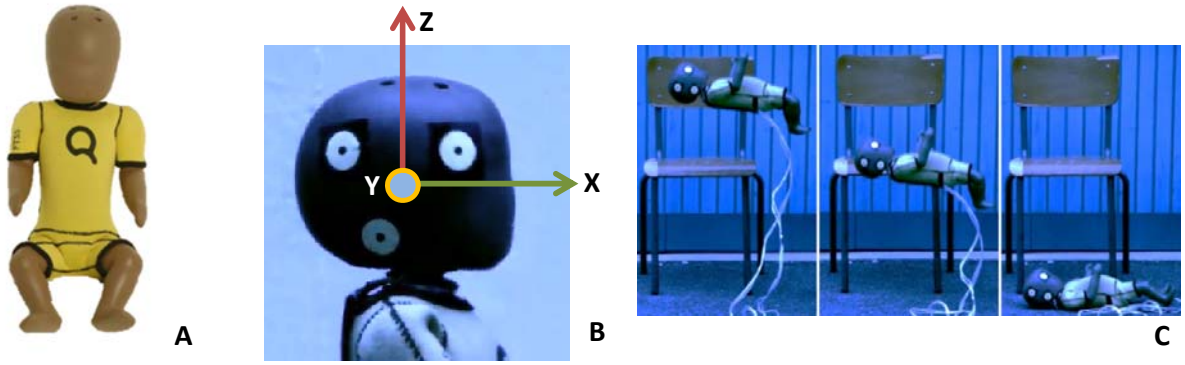

Fig. 1. A - Q0 dummy: a six weeks old newborn, B - Axis of the accelerometer in the dummy head, C - Images at three different states during the 130cm fall onto concrete.

TABLE I
Q0 DUMMY EXPERIMENTS

Height	Surface	Label
45 cm	Grass	Impact 1
45 cm	Linoleum	Impact 2
45 cm	Concrete	Impact 3
Backward impact	Wall	Impact 4
130 cm	Concrete	Impact 5

Computational Modelling

The infant eye model was generated by using globe and inner component dimensions from [5], location and diameter of the optic nerve from [14], muscles insertions, widths and lengths from [15] as illustrated in Fig. 2-3. Finally, from MRI data of a five month old female baby, infant globe and orbital wall dimensions were assessed and a scaling of 0.89 was applied to the adult based geometry. The orbital wall was generated afterwards. Muscles have been assigned a thickness of 2 mm. The optic nerve was generated by linking the globe straightly to the apex of the orbital wall (Fig. 5 B).

Except the retina, choroid, front membrane, orbital wall and the trochlea which were meshed with shell elements (quads or triangles), all other components were meshed with solid elements (hexahedron or pentahedron). Mesh continuity was carefully respected, except at the junction between the inferior oblique (IO) muscle and the orbital wall and for the orbital fat. Due to the network formed by the muscles and optic nerve, the fat component has a very irregular shape. This problem was handled by meshing the empty space between the globe and the orbital wall, and then by manually removing elements interfering with the muscles and optic nerve. With this solution, the mesh of the fat is in continuity with the globe and with the orbital wall, but there is no contact with the muscles and optic nerve (Fig. 4 C). The fully meshed model contains 45,154 elements, among which 4,644 are shell elements (Fig. 4 B, Fig. 5).

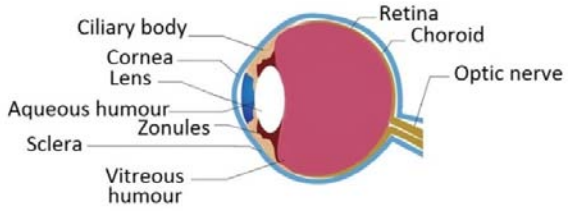

Fig. 2. Anatomy of globe inner components

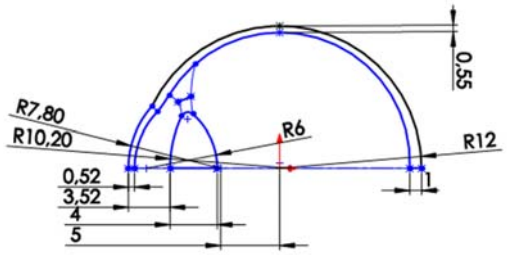

Fig. 3. Eye components dimensions [5]

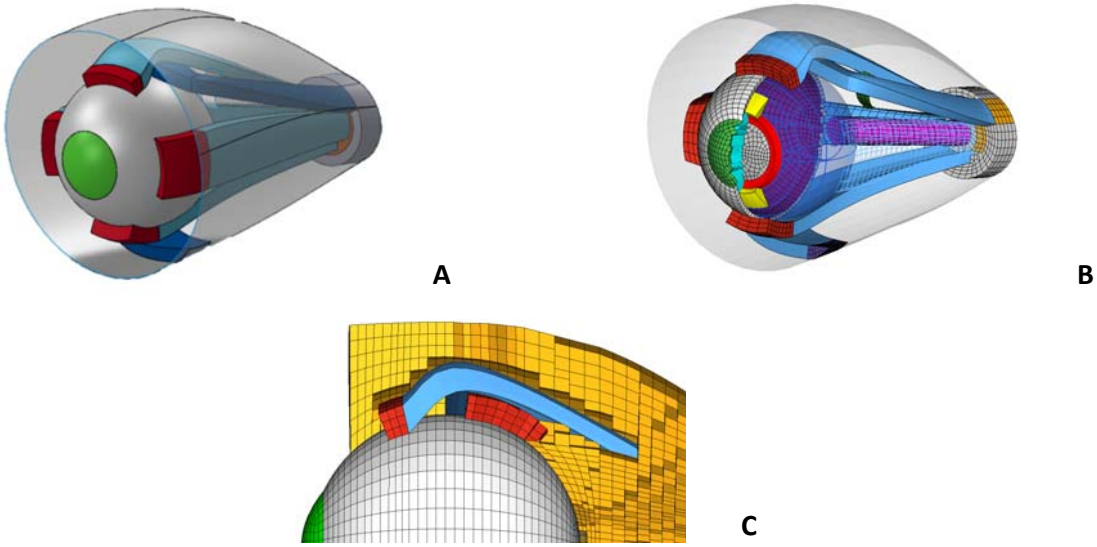

Fig. 4. A – CAD model of the infant eye, B – Mesh of the CAD model, C – Details of the mesh of the fat component

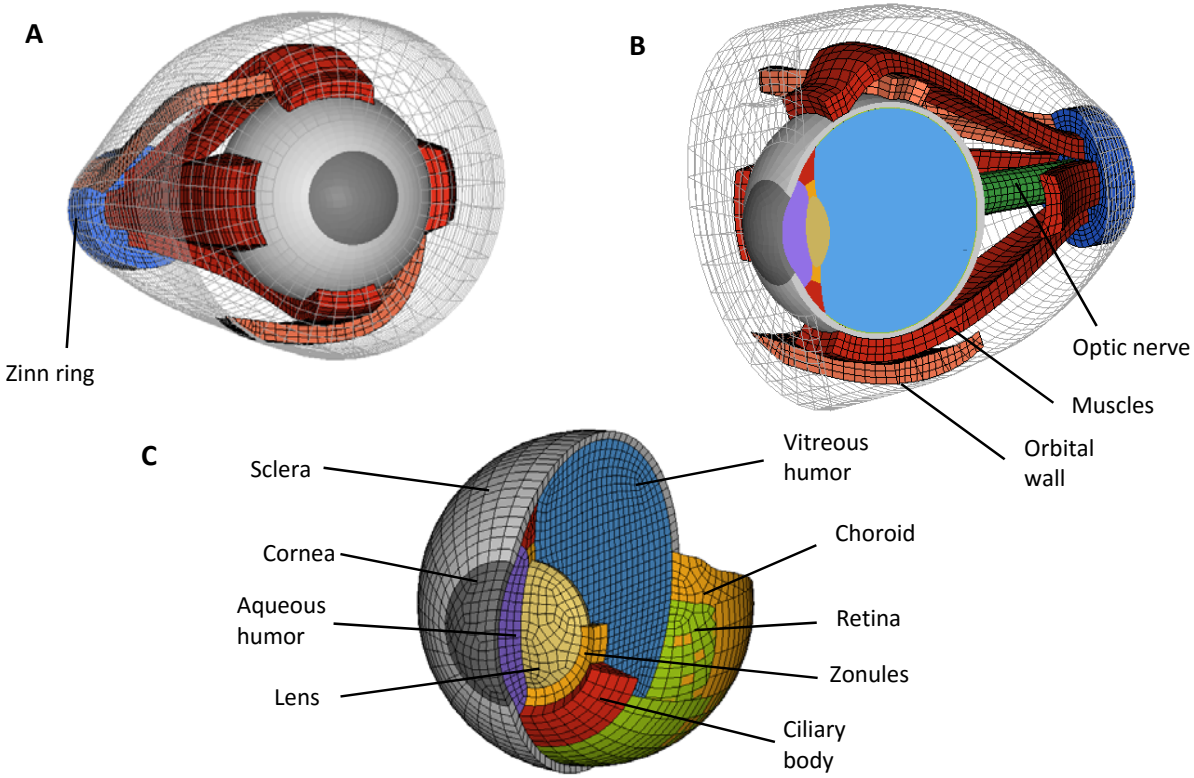

Fig. 5. Different views of the developed infant eye FEM : A - whole model; B - cross section view; C - inner globe components.

A literature review of eye component mechanical properties has been conducted in order to identify the most biofidelic material property for each part. A total of three types of law were considered, i.e. two non-linear (Mooney-Rivlin and Viscoelastic) and one linear (Elastic). Mooney-Rivlin law is derived from the two parameter strain-energy function and was used for the sclera, cornea and orbital fat, according to data provided in [8][16-17] respectively. The gel-like vitreous component was modelled with a viscoelastic law from [13].
All other components were modelled by a linear elastic law with Young's modulus from the literature. Retina and choroid Young's modulus were computed from the non-linear stress-strain curves provided in [18]. As no data on the mechanical properties of the Zinn ring exist in the literature, the value of 870 MPa was selected as its Young's modulus from a study on the human Achilles tendon [19]. The same problem was faced for eye muscles for which data from experiments on the rat tail was used as suggested in [20]. Orbital wall and trochlea were defined as rigid materials. The finalized FEM of the infant eye has a mass of 32.7 g.

Table 2 summarizes the mechanical parameters implemented in the developed infant eye FEM in LS-Dyna.

Two types of contacts have been used in LS-Dyna: *CONTACT_TIED_NODES_TO_SURFACE_OFFSET contact for fat/muscles, fat/optic nerve, IO muscle/orbital wall and *CONTACT_AUTOMATIC_SURFACE_TO_SURFACE contact between muscles, superior oblique muscle and sclera.

TABLE II
SUMMARY OF INFANT EYE FEM MECHANICAL PARAMETERS
E is the Young's modulus (kPa), G_0 and G_∞ are the initial and long-term shear modulus (kPa), B is the decay coefficient (s^{-1}), K is the bulk modulus (kPa), A and B are the Mooney-Rivlin parameters.

Component	Element type	Number ofelements	Type of law	ρ (kg/m^3)	ν	Parameters	References
Sclera	Brick	1531	Mooney-Rivlin	1243	0.49	A = 495 B = -470.2	[16]
Cornea	Brick	172	Mooney-Rivlin	1076	0.42	A = -63 B = 86.69	[8]
Orbital fat	Brick	16812	Mooney-Rivlin	1800	0.4	A = -5 B = 7.1	[17]
Vitreous	Brick	13475	Viscoelastic	1009		G_0 = 0.01 kPa G_∞ = 0.0003 kPa B = 14.26 s^{-1} K = 2e+6 kPa	[13]
Aqueous	Brick	713	Elastic	1003	0.49	E = 0.043 kPa	[12]
Lens	Brick	342	Elastic	1078	0.49	E = 6880 kPa	[5]
Zonules	Brick	160	Elastic	1000	0.4	E = 582 kPa	[21]
Ciliary body	Brick	520	Elastic	1600	0.4	E = 582 kPa	[21]
Retina	Shell	931	Elastic	1000	0.49	E = 11 kPa	[18]
Choroid	Shell	1251	Elastic	1000	0.49	E = 159 kPa	[18]
Optic nerve	Brick	1012	Elastic	1000	0.47	E = 5.5 kPa	[11]
Eye muscles	Brick	4808	Elastic	1600	0.4	E = 11000 kPa	[20]
Zinn Ring	Brick	965	Elastic	1000	0.49	E = 8.7e+5 kPa	[19]
Membrane	Shell	320	Elastic	1000	0.46	E = 150 kPa	[12]
Orbital wall and trochlea	Shell	2142	Rigid	1900	0.21	-	[22]

In order to reproduce the experimental impacts conducted with the Q0 dummy, the eye model was oriented as in a backward fall and the recorded uniaxial accelerations (along X axis) were assigned to the rigid orbital wall. Furthermore, as the dummy head response is not direction dependent, the sensitivity of the model was studied by orienting it to simulate lateral and frontal impacts with the same recorded accelerations. Finally, for each simulation, five parameters (pressure, principal stress, principal strain, Von Mises stress and Von Mises strain) were computed for all eye components.

III. RESULTS

To investigate RH in infants after falls, realistic falls were reproduced with an infant dummy and were used as inputs for the infant eye FEM. This section presents the results of the experimental and numerical parts.

Experimental drop results show that for the same height of 45 cm, the maximum accelerations grow when the surface becomes harder and range from 110 to 394 g, and the duration of the pulse is smaller in case of harder surfaces (Fig. 6). Results in terms of HIC15 range from 151 to 1,747. It is important to notice that even though for Impact 1 to 3, the acceleration is only 3.5 higher, and HIC15 value is more than 10 times higher. With the same concrete surface, the variation of height induces a higher maximum acceleration: from 394 g to 687 g, with a peak HIC15 of 6,027. Here, the ratios for the accelerations and for HIC15 values were not much different: 1.7 and 3.4 respectively. Impact experiment against a wall generates a peak acceleration of 556 g and a HIC15 of 3,399: those values are between a concrete fall from 45 cm and 130 cm (Table III, Fig. 7). Table III presents the simulation matrix with results in terms of maximum acceleration, duration and HIC15. Fig. 6 shows the obtained

acceleration curves and Fig. 7 compares maximum accelerations and HIC15 values. As a whole, this values show that maximum accelerations are only poorly correlated with HIC15.

TABLE III
Q0 DUMMY EXPERIMENTS RESULTS

Label	Height	Surface	Max acc (G)	Duration (ms)	HIC15
Impact 1	45 cm	Grass	110	4	151
Impact 2	45 cm	Linoleum	349	3	1336
Impact 3	45 cm	Concrete	394	3	1747
Impact 4	Backward impact	Wall	556	1.8	3399
Impact 5	130 cm	Concrete	687	2	6027

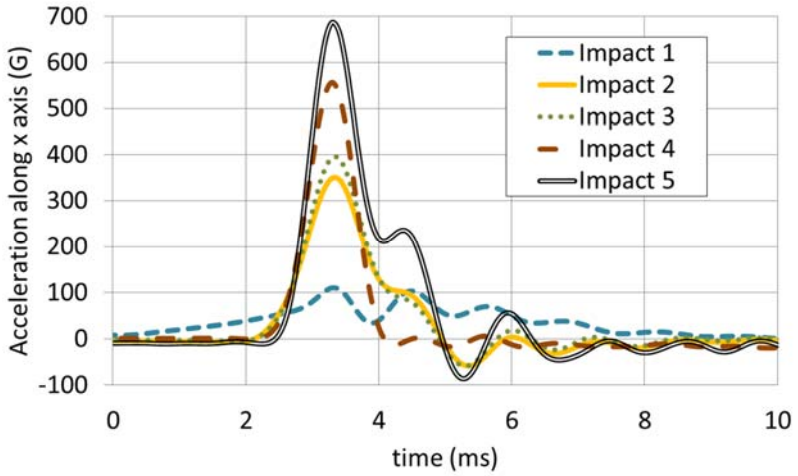

Fig. 6. Acceleration along X axis (G) versus time curves for each experiments

From each simulation, five parameters, i.e. Pressure, Principal stress, Principal strain, Von Mises stress and Von Mises strain were computed for all eye components. As the study is about RH, the focus was put on the retina component.

Results of the simulations are sumarized for each of the five parameters in Fig. 8-10. The general tendency is that for each orientation, maximum values of parameters were ordered in the same way as acceleration and HIC15 as shown in Fig. 7. Among the three head orientations, frontal impacts show the highest computed intra-ocular parameters. Again, as for maximum accelerations, it appears that intra-ocular parameters are only poorly correlated with HIC15. Moreover, for Impact 1 which presents a low acceleration but a long duration, intra-ocular parameters are of similar order as for Impact 2. The Impact 1 leads also to significantly higher shearing stress and strain in case of lateral impact.

For occipital impacts, the Von Mises stress and maximum pressure parameters had the most significant increase between Impact 1 to 5, with a ratio of 3.5. For frontal impacts, that parameter is the minimum pressure with a ratio of 8.6. For lateral impacts the situation is different as for the pressure, Von Mises stress and strain, values for Impact 1 were even greater than for Impact 4. The ratio between Impact 1 and 5 is the same for both principal strain and stress in the lateral orientation. Simulation results and ratios are available in Tables 4-5-6.

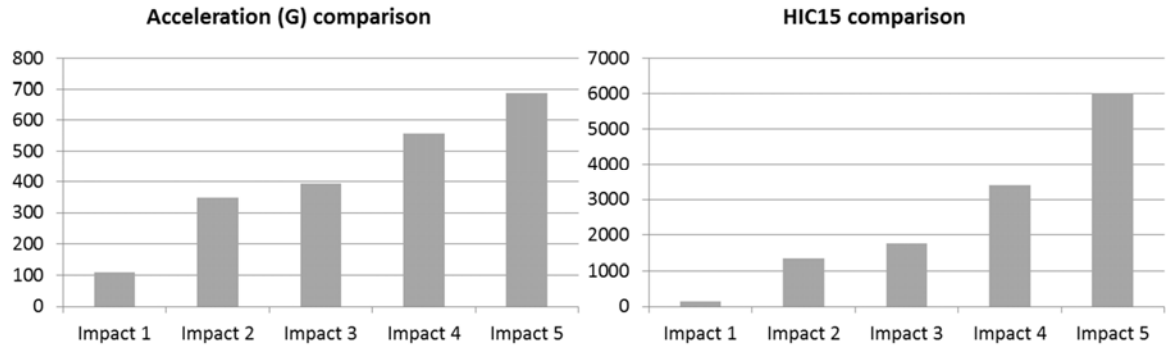

Fig. 7. Acceleration (G) and HIC15 comparison for the 5 impacts.

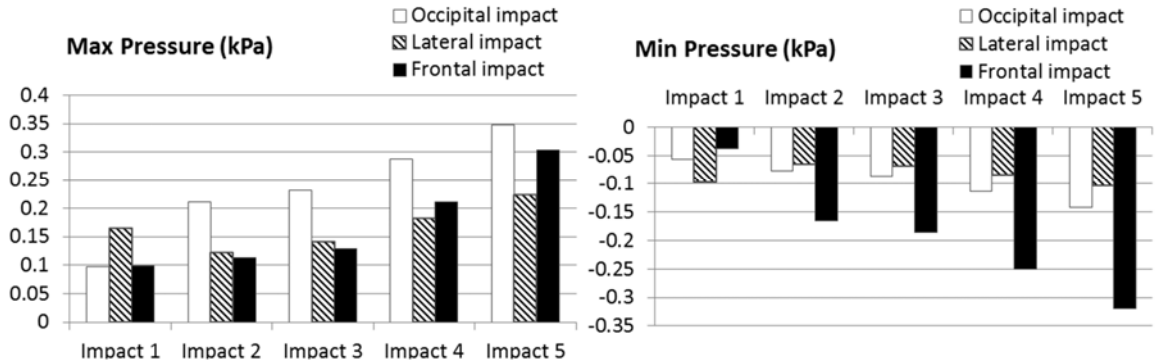

Fig. 8. Comparison between the three orientations for the Pressure parameter (minimum and maximum) in the retina.

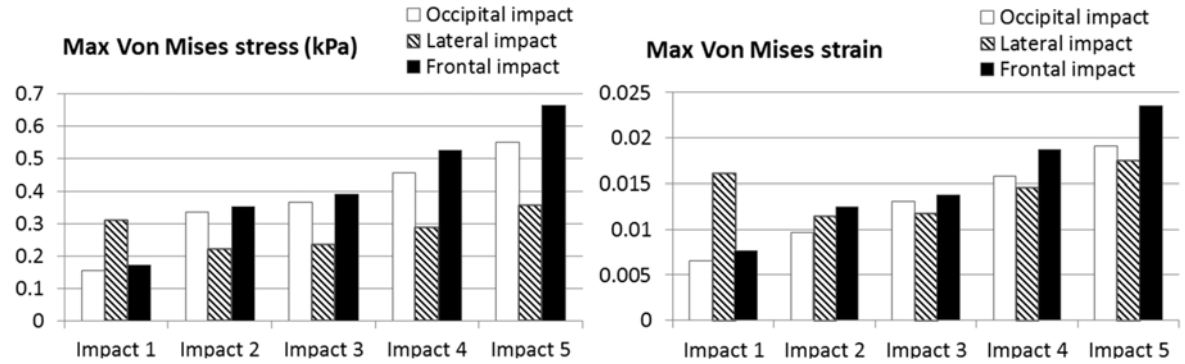

Fig. 9. Comparison between the three orientations for the Von-Mises stress and strain parameters in the retina.

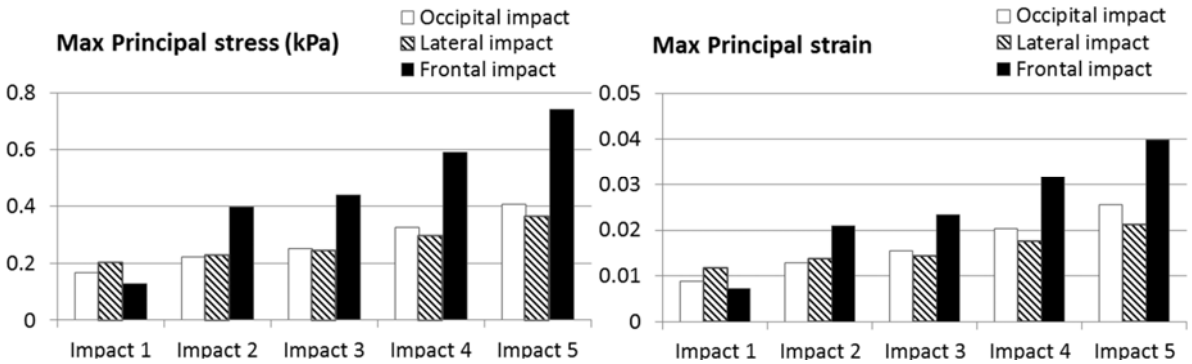

Fig. 10. Comparison between the three orientations for the Principal stress and strain parameters in the retina.

TABLE IV
SIMULATION RESULTS FOR THE OCCIPITAL ORIENTATION

Simulation	Max Pressure (kPa)	Min Pressure	Von Mises stress (kPa)	Von mises strain	Principal Stress (kPa)	Principal strain
Impact 1	0.097	-0.056	0.154	0.006	0.166	0.008
Impact 2	0.211	-0.077	0.334	0.009	0.221	0.012
Impact 3	0.231	-0.086	0.364	0.013	0.249	0.015
Impact 4	0.287	-0.113	0.453	0.015	0.324	0.021
Impact 5	0.347	-0.142	0.549	0.019	0.403	0.025
Ratio impacts 5/1	3.57	2.53	3.56	3.16	2.42	3.125

TABLE V
SIMULATION RESULTS FOR THE LATERAL ORIENTATION

Simulation	Max Pressure (kPa)	Min Pressure	Von Mises stress (kPa)	Von mises strain	Principal Stress (kPa)	Principal strain
Impact 1	0.165	-0.097	0.312	0.016	0.201	0.011
Impact 2	0.123	-0.066	0.221	0.011	0.229	0.013
Impact 3	0.141	-0.069	0.237	0.011	0.244	0.014
Impact 4	0.183	-0.085	0.289	0.014	0.297	0.017
Impact 5	0.225	-0.104	0.359	0.017	0.365	0.021
Ratio impacts 5/1	1.36	1.07	1.15	1.06	1.81	1.91

TABLE VI
SIMULATION RESULTS FOR THE FRONTAL ORIENTATION

Simulation	Max Pressure (kPa)	Min Pressure	Von Mises stress (kPa)	Von mises strain	Principal Stress (kPa)	Principal strain
Impact 1	0.099	-0.037	0.171	0.007	0.129	0.007
Impact 2	0.113	-0.165	0.351	0.012	0.394	0.021
Impact 3	0.128	-0.186	0.391	0.013	0.439	0.023
Impact 4	0.212	-0.250	0.524	0.018	0.588	0.031
Impact 5	0.303	-0.320	0.662	0.023	0.741	0.039
Ratio impacts 5/1	3.06	8.64	3.87	3.28	5.74	5.57

IV. DISCUSSION

To investigate RH in infants following head impact, an infant eye FEM was developed. With acceleration data recorded from Q0 dummy experimental impacts against different surfaces and different heights, eye response simulations were performed under occipital, lateral and frontal impact conditions. It is important to note that to study blunt impact to the eye, authors in [5] have used an ALE (Arbitrary Lagrangian-Eulerian) method: this method is indeed relevant in case of high deformation or flow in the fluid-structure interface. In this study, as falls are not supposed to produce such deformation or flow and in order to reduce the computation time, a traditional Lagrangian approach was chosen.

Impact experiments have been conducted at 45 cm (grass, linoleum, concrete) and 130 cm (concrete only). The 45 cm height corresponds to an adult sitting on a chair or the height of a bed. The 130 cm is higher than a baby changing table which is more likely to be 100 cm, but it corresponds to an adult holding a baby in their arms. These heights were estimated to be relevant to analyze outcomes of what can be qualified as domestic falls. The rear impact on wall (Impact 4) is not a domestic fall, but was performed to mimic child abuse and to have an idea of the acceleration sustained in such situation. The selected impact conditions also occur in traffic accidents when the child head impacts interior car structures.

Experimental results show clearly that the 130 cm fall height onto concrete produces the highest acceleration and HIC15 values. Though, one could have estimated the wall impact HIC15 value of 3,399 (Impact

4) to be closer to the 130 cm fall (Impact 5) HIC15 value of 6,027: this demonstrates the importance of the acceleration pulse duration in impacts. The opposite trend was noticed for Impacts 2 and 3: similar maximum accelerations and pulse durations lead to close HIC15 values (Table 3). Without any surprise, falls on grass generated the lowest acceleration and HIC15 values (Fig. 4) which point out grass damping property compared to other surfaces.

In the literature, few studies have established thresholds based on HIC for injuries (skull fracture and AIS3) based on injury risk tolerance scaling or on reconstruction of child cadaver experiments [23-24]. The proposed HIC15 values for a 50% skull fracture or risk of AIS3 are between 290 and 671. In the present study, the fall from 45 cm onto grass is the safest one as the associated HIC15 value is 151 whereas Impact 4 and 5 are the worst with values 5 to 10 times higher than those thresholds. Although the cited limits have not been established for RH, it can be reasonably hypothesized that RH may appear in such extreme cases.

Based on the experiments, five simulations were performed to replicate an occipital impact. The FEM was then oriented and the same set of accelerations were used to simulate lateral and frontal impacts. This allowed the evaluation of the influence of head orientation.

For each orientation, the fall from 130 cm induced the highest value for each of the five computed parameters whereas impact on grass induced the lowest values. For each parameter, the frontal impact generated the highest values, except for the Maximum Pressure, for which the occipital impact was the most critical and the lateral orientation seems to be the safest. Among impacts, it was noticed that Impact 2 and 3 have similar HIC15 values: this resulted in similar values for the five parameters.

The trend seen in lateral impacts was noticed and thus the results must be taken with care: indeed for some parameters, maximum values for Impact 1 are much higher than for Impact 2, 3 and 4. This is likely to be a numerical artifact as this behavior could not be seen during other impacts or in the two other orientations.

As mentioned in the results section, among the five parameters it was not possible to select a relevant one, but only possible to show that the Von Mises stress, the principal stress/strain and the pressure have the highest increase from Impact 1 to Impact 5, as shown in Tables 4, 5 and 6 with the ratios.

In the literature, there is no established threshold for RH. However, in [13] the authors suggested a limit for retinal detachment in terms of pressure, between retina and choroid, at 340 Pa by conducting experiments on living rabbit eyes. This threshold has clearly no direct link with RH. The main reason for including this control parameter is that it is the only mechanical parameter which can be experimentally recorded. The results of this study are compared to this limit in order to understand the level of loading inside the eye during the considered impact situations: the threshold was almost reached during Impact 4 (287 Pa) and was exceeded for Impact 5 (Fig. 11).

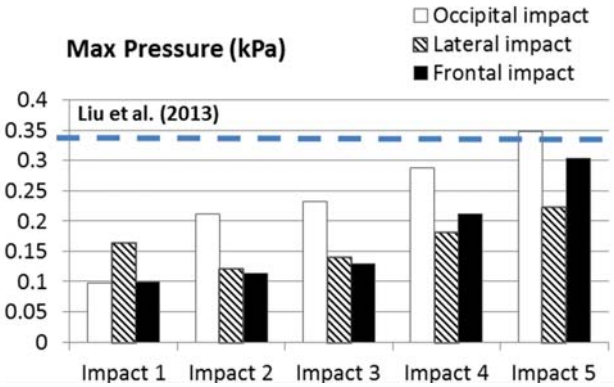

Fig. 11. Comparison of simulation results and threshold established in [13] for retinal detachment in terms of pressure in the retina.

The limitations of this study lie mainly in the numerical approach. The first aspect is the geometry: the presented infant eye is only a uniform scale down of an adult one and thus can be questioned. Material properties were taken from either human adults or animals and most of the time the testing was performed in vitro. Concerning the experimental aspects, the impacts were directed along the head CG so that no or very

limited head rotation occurs. In further investigation, the rotational acceleration of the head should be recorded and adequate eye acceleration should be calculated. Moreover, for the orientation study, the same occipital impact accelerations were used for the lateral and frontal simulations: for the same height and surface, occipital and lateral impacts are not likely to give the same acceleration profile. The orientation study presented here is therefore only a preliminary step to understand the behavior of the eye. Finally, a recurrent problem for FEM of children eyes is the validation step. In the literature, only [5] proposed a quantitative validation protocol by comparing globe impact videos and areas of the sclera under high stress/strain.

Finally this pilot study does not consider thresholds for eye injury, but provides a tool to progress in the field. In a further step well documented road accidents but also domestic accidents as well as cases from legal medicine should be simulated in order to correlate the different intra-ocular mechanical parameters with the occurrence of injury.

V. CONCLUSIONS

A set of experimental child dummy impacts were conducted under different impact conditions in order to record the head acceleration. On the other hand a detailed infant eye FEM was developed with updated material properties. This allowed conducting numerical simulation of the eye response in case of falls on the occipital, lateral and frontal areas. Results in terms of intra-ocular parameters show clearly that among impacts, the fall from 130 cm is the one producing the highest values whereas among orientations, frontal impacts are the ones producing the highest values. In a further step, documented fall reconstructions will help to establish an injury threshold for retinal haemorrhages for infants to be applied in child safety system design.

VI. REFERENCES

[1] Laurent-Vannier A, Nathanson M, et al. A public hearing « Shaken baby syndrome: Guidelines on establishing a robust diagnosis and the procedures to be adopted by healthcare and social services staff ». Guidelines issued by the Hearing Commission. *Annals of Physical and Rehabilitation Medicine*, 2011, 54:600-625.

[2] Levin AV. Vitreoretinal traction is a major factor in causing the hemorrhagic retinopathy of abusive head injury – yes. *Eye*, 2009, 23:1758-1760.

[3] Clarke MP. Vitreoretinal traction is a major factor in causing the hemorrhagic retinopathy of abusive head injury – No. *Eye*, 2009, 23:1761-1763.

[4] Wygnanski-Jaffe T, Levin AV, et al (2006) Postmortem Orbital Findings in Shaken Baby Syndrome. *Am J Ophthalmol*, 2006, 142:233–240.

[5] Stitzel JD, Duma SM, Cormier JM, Herring IP. A nonlinear finite element model of the eye with experimental validation for the prediction of globe rupture. *Stapp Car Crash Journal*, 2002, 46:81-102.

[6] Rossi T, Boccassini B, et al. Primary Blast Injury to the Eye and Orbit: Finite Element Modeling. *Invest Ophthalmol Vis Sci*, 2012, 53:8057-8066.

[7] Bocskai Z, Bojtár I. Biomechanical modelling of the accommodation problem of human eye. *Period Polytech Civ Eng*, 2013, 57:3.

[8] Uchio E, Ohno S, Kudoh J, Aoki K, Kisielewicz LT. Simulation model of an eyeball based on finite element analysis on a supercomputer. *Br J Ophthalmol*, 1999, 83:1106-1111.

[9] Cirovic S, Bhola RM, Hose DR, Howard IC, Lawford PV, Parsons MA. Mechanistic hypothesis for eye injury in infant shaking. *Forensic Sci Med Pathol*, 2005, 1:53-59.

[10] Cirovic S, Bhola RM, Hose DR, Howard IC, Lawford PV, Parsons MA. A Computational study of the passive mechanisms of eye restraint during head impact trauma. *Comput Methods Biomech Biomed Engin*, 2005, 8:1-6.

[11] Cirovic S. Computer modelling study of the mechanism of optic nerve injury in blunt trauma. *Br J Ophthalmol*, 2006, 90:778-783.

[12] Hans SA, Bawab SY, Woodhouse ML. A finite element infant eye model to investigate retinal forces in shaken baby syndrome. *Graefes Arch Clin Exp Ophthalmol*, 2009, 247:561-571.

[13] Liu X, Wang L, Wang C, Sun G, Liu S, Fan Y. Mechanism of traumatic retinal detachment in blunt impact: A finite element study. *J Biomech*, 2013, 46:1321-1327.

[14] Kim H, Yoo L, Shin A, Demer JL. Determination of Poisson Ratio of Bovine Extraocular Muscle by Computed X-Ray Tomography. *BioMed Res Int*, 2013, 2013:1-5.

[15] Villarreal-Silva EE, Amaya JM, Cruz JJ, Fernandez DM, Elizondo-Omana RE, Lopez SG. A morphometric study of the extraocular muscles. *Int J Morphl*, 2013, 31(1):312-320.

[16] Bisplinghoff JA, McNally C, Manoogian SJ, Duma SM. Dynamic material properties of the human sclera. *J Biomech*, 2009, 42:1493-1497.

[17] Chen K, Weiland JD. Mechanical properties of orbital fat and its encapsulating connective tissue. *J Biomech Eng*, 2011, 133:064505.

[18] Chen K, Rowley AP, Weiland JD, Humayun MS. Elastic properties of human posterior eye. *J Biomed Mater Res A*, 2013, 102:2001-2007.

[19] Lichtwark GA. In vivo mechanical properties of the human Achilles tendon during one-legged hopping. *J Exp Biol*, 2005, 208:4715-4725.

[20] Power ED. A nonlinear finite element model of the human eye to investigate ocular injuries from night vision goggles. 2001, Dissertation, Virginia Polytechnic Institute and State University.

[21] Michael R, Mikielewicz M et al. Elastic Properties of Human Lens Zonules as a Function of Age in Presbyopes. *Invest Ophthalmol Vis Sci*, 2012, 53:6109-6114.

[22] Robbins DH, Wood JL. Determination of mechanical properties of the bones of the skull. *Experimental mechanics*, 1969, 9:236-240.

[23] Wismans et al. Q-dummies report - Advanced child dummies and injury criteria for frontal impact. *European enhanced vehicle-safety committee*, 2008.

[24] Van Ee C, Moroski-Browne B, Raymond D, Thibault K, Hardy W, Plunkett J. Evaluation and refinement of the CRABI-6 anthropomorphic test device injury criteria for skull fracture. *Proceedings of the ASME 2009 International Mechanical Engineering Congress & Exposition*, 2009, Florida, USA.